Bioactive Materials 6 (2021) 963–974

Contents lists available at ScienceDirect

Bioactive Materials

journal homepage: http://www.keaipublishing.com/biomat

Folic acid-modified Exosome-PH20 enhances the efficiency of therapy via modulation of the tumor microenvironment and directly inhibits tumor cell metastasis

Chunxiang Feng[a,b], Zhiyong Xiong[b], Cheng Wang[b], Wen Xiao[b], Haibing Xiao[a], Kairu Xie[a], Ke Chen[b], Huageng Liang[b], Xiaoping Zhang[b,**], Hongmei Yang[a,*]

[a] Department of Pathogenic Biology, School of Basic Medicine, Tongji Medical College, Huazhong University of Science and Technology, Wuhan, 430030, China
[b] Department of Urology, Union Hospital, Tongji Medical College, Huazhong University of Science and Technology, Wuhan, 430022, China

ARTICLE INFO

Keywords:
Hyaluronidase
Exosomes
Tumor microenvironment
Metastasis
Tumor immunotherapy

ABSTRACT

High accumulation of hyaluronan (HA) in the tumor microenvironment leads to an increase in the interstitial pressure and reduction perfusion of drugs. Furthermore, high molecular-weight (HMW)-HA suppresses M1 macrophage polarization, enhances M2 polarization, and induces immunosuppression. Hyaluronidase treatment have attempted to decrease the quantity of HA in tumors. However, hyaluronidase-driven HA degradation driven accelerates tumor cell metastasis, which is a major cause of mortality in cancer patients. Thus, we designed a novel exosome-based drug delivery system (DDS), named Exos-PH20-FA, using genetic engineering to express human hyaluronidase (PH20) and self-assembly techniques to modify the exosomes with folic acid (FA). Our results show that Exos-PH20-FA degraded HMW-HA to low-molecular-weight (LMW)-HA. Moreover, LMW-HA polarized macrophages to the M1 phenotype and reduced the number of relevant immunosuppressive immunocytes which changed the immune microenvironment from an immunosuppressive to immunosupportive phenotype. Furthermore, we demonstrated Exos-PH20-FA directly reduced hyaluronidase-induced metastasis of tumor cells. This tumor treatment also allowed an enhanced delivery of chemotherapy by tumor-targeting effect with FA modification. Our findings indicate that Exos-PH20-FA improves tumor treatment efficiency and reduces the side effects of hyaluronidase treatment, namely tumor cell metastasis. This all-in-one exosome-based HA targeting DDS maybe a promising treatment that yields more efficient and safer results.

1. Introduction

The accumulation of hyaluronan (HA) is common in a wide range of solid tumors, such as those of the breast, pancreas, colon, ovary, and prostate [1]. Furthermore, the HA content is usually higher in malignant tumors than in the corresponding benign tumors or normal tissues, and a high concentration of HA is associated with poor prognosis [2]. In tumors and normal tissues, HA mainly occurs as high molecular-weight (HMW)-HA (mass > 1000 kDa), a long-chain polysaccharide with repeating polymeric disaccharides [3]. One of the major functions of HA appears to be linked to immune surveillance [4]. Usually, HMW-HA suppresses M1 macrophage polarization and enhances M2 polarization via CD44 [5,6]. In response to tissue injury, HMW-HA is rapidly degraded by hyaluronidases or reactive oxygen species into low molecular-weight (LMW)-HA (mass < 200 kDa) that activates immunostimulatory activity [7]. LMW-HA has been shown to act as a damage-associated molecular pattern (DAMP), interacting with dendritic cells or endothelial cells via Toll-like receptor (TLR) 2/4 to initiate a proinflammatory response [8].

Preclinical studies demonstrate that hyaluronidase treatment can improve anticancer therapies effect [9,10]. Until now, many studies have focused on hyaluronidase treatments aiming to increase the tumor perfusion of chemotherapy drugs by improving the tumor microenvironment (TME) [11,12] or on the stimulated dendritic cells combined with PD-L1 blockade to boost antitumor-immunity [13]. However, the effect of hyaluronidase on tumor-associated macrophages (TAMs) polarization has not been studied in the context of antitumor therapy. TAMs account for a substantial proportion of tumor-infiltrating immune cells [14], and most TAMs present a pro-tumorigenic M2-like phenotype, which leads to the secretion of immunosuppressive cytokines, and recruitment of regulatory T cells (Tregs) to the tumor [15]. In turn, the accumulation of

Peer review under responsibility of KeAi Communications Co., Ltd.
* Corresponding author.
** Corresponding author.
E-mail addresses: xzhang@hust.edu.cn (X. Zhang), qingyang68@hotmail.com, hyang@HUST.edu.cn (H. Yang).

https://doi.org/10.1016/j.bioactmat.2020.09.014
Received 6 July 2020; Received in revised form 24 August 2020; Accepted 15 September 2020

these immunosuppressive immunocytes result in tumor invasion, and T cell suppression [16]. Therefore, it is necessary to reverse intra-tumoral immunosuppression during tumor treatment, and elevated HMW-HA and M2-like TAMs are promising targets of treatment.

Nevertheless, HA degradation during extracellular matrix (ECM) remodeling can enhance cancer cell migration and metastasis [17]. In metastatic patients, it is observed increased plasma LMW-HA levels which is due to the degradation of HMW-HA in ECM [18]. Furthermore, some targets or approaches of cancer treatments, such as macrophage inhibitory cytokine-1 or TME improvement by antiangiogenic therapy, limit local tumor growth but concomitantly promote metastases in some cases [19,20]. Since, metastasis is the primary cause of morbidity and mortality in patients with advanced cancer, as well as a side effect of hyaluronidase treatment, the dual effect of hyaluronidase as cancer therapy needs to be taken into account. In this study, we for the first time sought to develop a strategy of hyaluronidase treatment to reverse immunosuppression, while minimizing its side effect of tumor cell metastasis which triggered by hyaluronidase. Folic acid (FA) has a natural high binding affinity for FA receptors, whose expression is much higher on the surface of tumor cells than on the surface of normal cells [21]. Therefore, FA-modified drug delivery system (DDS) are often used to deliver chemotherapeutic agents to cancer cells and facilitate their uptake by the tumors. Moreover, FA can inhibit tumor cell migration by FA receptor/cSrc-signaling pathway and without affecting cellular activity [22].

Thus, in this study, we sought to develop a hyaluronidase treatment strategy that reverses immunosuppression, enhances tumor targeting, and minimizes hyaluronidase-triggered tumor cell metastasis. To this end, we developed a self-assembly and genetically engineered exosome-based DDS expressing human hyaluronidase (PH20) and FA, named Exos-PH20-FA. Our results show that PH20 in our DDS degraded tumor stromal HMW-HA into LMW-HA, which reoriented pro-tumorigenic M2-like TAMs to anti-tumorigenic M1-like TAMs. Moreover, Exos-PH20-FA not only improved the efficacy of a treatment combining chemotherapy but also directly reduced the risk of tumor cell metastasis caused by hyaluronidase (Fig. 1). Based on our findings, we envision that this system may be more suitable for HA^{hi} tumor treatment than other previously reported systems.

2. Materials and methods

2.1. Materials

The recombinant plasmid encoding PH20 was provided by VectorBuilder (Guangzhou, China). Lipofectamine 3000 was obtained from Invitrogen (USA). 1,2-Distearoyl-*sn*-glycero-3-phosphoethanolamine - N - [folate(polyethylene glycol)] (DSPE-PEG-FA) was provided by Ponsure Biological (Shanghai, China). PH20 was obtained from Rhinozyme (Soochow, China). PKH67 and phalloidin-rhodamine were obtained from Sigma-Aldrich (USA). DiR was provided by Thermo Fisher Scientific (USA). Fetal bovine serum (FBS), RMPI 1640 and DMEM medium were obtained from Gibco (USA). MTT was provided by Servicebio (Wuhan, China). HMW-HA extracted from rooster comb was provided by Sigma (USA).

2.2. Cell culture

The human prostate cancer cell line PC3, normal cell line HEK 293T, human kidney proximal tubule cell line HK-2, mouse breast cancer cell line 4T1, and luciferase (Luc)-labeled 4T1 cells were purchased from the Cell Bank of the Chinese Academy of Sciences (Shanghai, China). HEK 293T cells were maintained in DMEM supplemented with 10% exosome-free FBS, and PC3 and 4T1 cells were maintained in RMPI 1640 medium supplemented with 10% FBS, HK-2 cells were maintained in DMEM supplemented with 10% FBS. All cell lines were cultured in a 5% CO_2 incubator at 37 °C. Bone-marrow-derived macrophage cells (BMDMs) were extracted from leg bones of BALB/c mice, and cells were maintained in DMEM supplemented with 10% FBS and 1% antibiotic-antimycotic. For differentiation into Mø macrophages, BMDMs were treated with 20 ng/mL murine M-CSF for 7 days. For differentiation into M2 macrophages, Mø macrophages were treated with 20 ng/mL murine IL-4 for 24 h.

2.3. Exosome preparation and isolation

The engineered recombinant plasmid encoding PH20 was transfected into HEK 293T cells using Lipofectamine 3000 according to the manufacturer's instructions. To establish stably transfected cells, the latter were selected with 2 μg/mL puromycin for 2 weeks. The fluorescence of PH20-expressing HEK 293T cells was observed by immunofluorescence staining with anti-PH20 (1:100, ABclonal Technology, China) with Ti–S microscope (Nikon Instruments, USA). The supernatants of PH20-overexpressing cells were harvested and centrifuged through multi-step gradient force to isolate exosomes [23], which were then resuspended in PBS and stored at −80 °C.

2.4. Preparation of FA-Modified exosomes and doxorubicin encapsulation

FA was incorporated into Exos-PH20 through the self-assembly insertion method [24]. Briefly, DSPE-PEG-FA was dissolved in DMSO, and then mixed with Exos-PH20 at a DSPE-PEG-FA:Exos protein weight ratio of 1:1. After 4 h of incubation at 37 °C, unincorporated (free) DSPE-PEG-FA was removed by ultrafiltration in a 300K Nanosep centrifuge (Pall Corporation, USA). Subsequently, doxorubicin (Dox) was loaded into the engineered exosomes by electroporation [25]. Briefly, Dox and the exosomes were mixed and suspended in electroporation buffers in a cuvette, electroporation was carried out at 350 μF and 250 V with the Gene Pulser Xcell electroporation system (Bio-Rad, USA), and the mixture was then incubated at 37 °C for 30 min to recover the exosomal membrane. The concentration of Dox encapsulated in Exos-PH20-FA was determined by UV–vis absorption spectroscopy (Beckman, USA) at 490 nm [26].

2.5. Evaluation of PH20 enzymatic activity and preparation of LMW-HA

To study the enzymatic activity of Exos-PH20 and Exos-PH20-FA, an enzymatic activity assay was performed as previously described [11]. Briefly, Exos-Con, Exos-PH20, Exos-PH20-FA, or PH20 were diluted in PBS, and then a hyaluronic acid solution was mixed with the samples and incubated at 37 °C for 45 min. An acidic albumin solution was added to the samples and incubated at 25 °C for 10 min. HMW-HA was mixed with albumin to form a clot (at acidic pH), which was detected at 600 nm by UV–vis spectrometry. HMW-HA was diluted to 5 mg/mL in 0.1 M sodium acetate buffer (pH 5.3), mixed with Exos-PH20, and incubated for 24 h at 37 °C. Digestions were stopped by inactivating the enzymes at 85 °C for 20 min. LMW-HA was acquired by ultrafiltration in a 10K Nanosep centrifuge and verified by Mass Spectrometer LC-MSD-Trap (Agilent, USA).

2.6. Characterization of the engineered exosomes

The morphology and size distribution of Exos-Con, Exos-PH20, and Exos-PH20-FA were characterized by transmission electron microscopy (TEM) (Hitachi, Japan) and Nano-ZEN 3600 (Malvern Instruments, UK) instruments. *Anti*-PH20 (1:500, ABclonal Technology) and the exosomal markers CD63 (1:1000, Santa Cruz Biotechnology, USA) and CD9 (1:1000, Santa Cruz Biotechnology) were used for detection by western blotting. Incorporation of FA in the engineered exosomes was confirmed by Fourier transform infrared (FTIR) spectrometry in the 400–4000 cm^{-1} range (VERTEX 70, BRUKER, Germany).

2.7. Establishing an orthotopic mouse model of 4T1 breast cancer

Animal protocols were approved by the Animal Research Committee of the Huazhong University of Science and Technology.

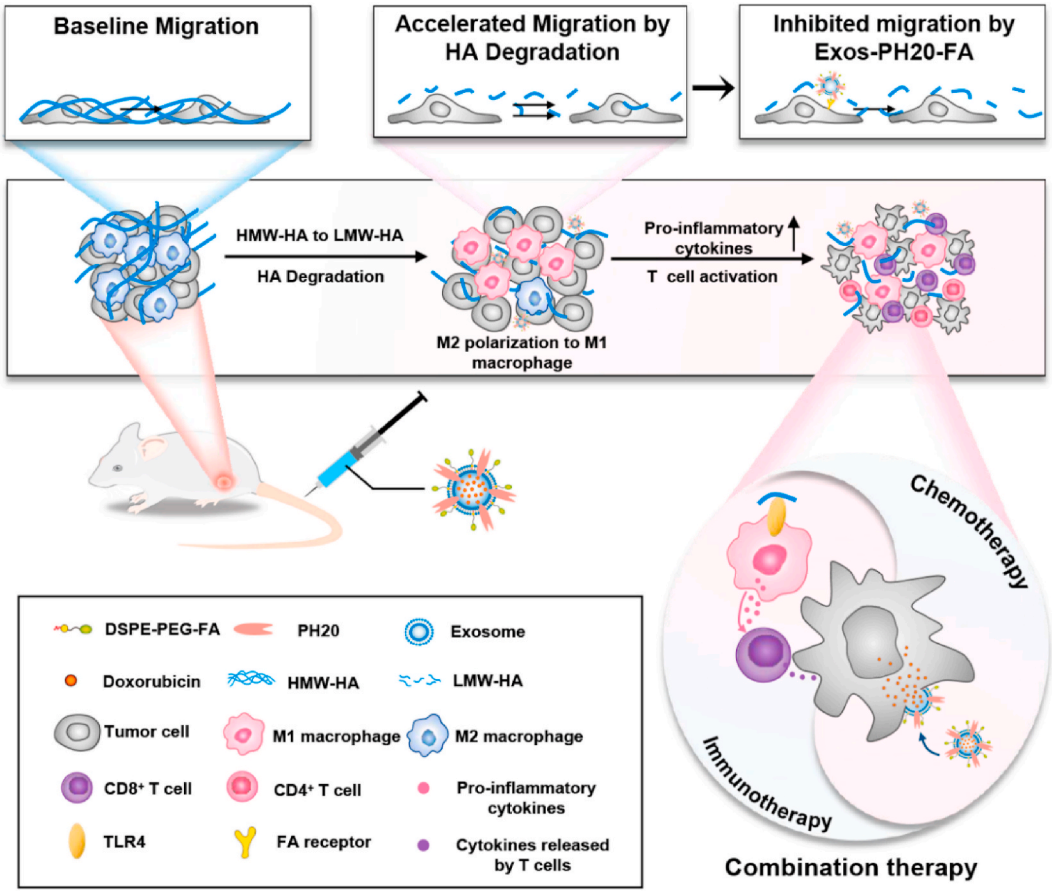

Fig. 1. Scheme illustration of the effects of Dox@Exos-PH20-FA on the modulation of the TME, which leads to enhanced DDS uptake by the tumor and conversion of the immune microenvironment from immunosuppressive to immunosupportive to favor cancer therapy. Furthermore, Exos-PH20-FA directly reduce the accelerated migration of tumor cells triggered by HA degradation.

Female BALB/c mice aged 6 weeks were purchased from the SLAC Laboratory Animal Company (Beijing, China). 4T1 murine breast cancer cells (1×10^6/100 μL) were injected into the mammary gland of mice. A digital caliper was used to investigate tumor growth every 2 days. The width (W) and length (L) of tumors were measured, and tumor volumes were calculated as (L × W × W)/2.

2.8. Evaluation of PH20 enzymatic activity and FA targeting effect of Exos-PH20-FA in vitro and in vivo

To assess the ability of the engineered exosomes to target PC3, 4T1, and HK-2 cells and degrade HA, cells were treated with culture medium containing Exos-Con, Exos-PH20, or Exos-PH20-FA (100 μg/mL), labeled with PKH67, a green fluorescent dye, according to the manufacturer's instructions. Cells were fixed in 4% paraformaldehyde and incubated with an anti-hyaluronic acid binding protein (HABP) antibody (1:100, ABclonal Technology) for 12 h at 4 °C and goat anti-mouse IgG (1:100, AmyJet Scientific, China) for 1 h at 37 °C, and cell nuclei were stained with 4′,6-diamino-2-phenylindole dihydrochloride.

To analyze the enzymatic activity of Exos-PH20-FA *in vivo*, we intratumorally injected Exos-Con, Exos-PH20, and Exos-PH20-FA (40 mg/kg) when the tumors reached 150–200 mm^3. After 24 h, tumor tissues were excised, fixed in 4% paraformaldehyde overnight, and analyzed for changes in the TME. To acquire scanning electron microscopy (SEM) images of the tumors, we gradually displaced paraformaldehyde with ethanol by immersing the tumor tissues in aqueous ethanol solutions of increasing ethanol concentrations. Tumors in 100% ethanol were dehydrated using a critical point dryer and metallized for SEM characterization. For immunohistochemical staining, the fixed tumor tissue was embedded in paraffin and sectioned, and sections were incubated with anti-HABP antibody (1:100, ABclonal Technology).

To assess the tumor-targeting ability of Exos-PH20-FA *in vivo*, exosomes were labeled with 5 μM DiR, a near-infrared fluorescent dye, for 30 min at 37 °C prior to intravenous injection. When orthotopic tumors reached 200–300 mm^3, 100 μL Exos-Con, Exos-PH20, or Exos-PH20-FA (1 mg/mL) were intravenously injected. The intensity of the fluorescent signal in mice was detected using a live imaging system (Lago X, SI Imaging) 12 and 24 h post-injection. The radiance (photons s^{-1} cm^{-2} sr^{-1}) of the regions of interest was quantified with the Living Image software. Mice were sacrificed after the 24 h imaging time point, and their major organs were collected for fluorescence imaging.

2.9. Investigation of tumor cell viability and cellular uptake of Dox loaded in exosomes

4T1 cells (1.0×10^4 cells/well) were seeded into a 96-well plate and cultured for 24 h. The culture medium was suctioned off, and cells were incubated with fresh medium plus PBS (blank control), free Dox, Dox@Exos-Con, Dox@Exos-PH20, or Dox@Exos-PH20-FA (Dox at 0.5, 1, 2, 4, and 8 μg/mL) for 12 h. The viability of 4T1 cells was evaluated by the MTT assay (n = 4). To evaluate the uptake of Dox by different carriers using flow cytometry (phycoerythrin channel, CytoFLEX, Beckman), we shortened the incubation time to 6 h.

2.10. In vitro measurement of TAMs polarization

For immune phenotype analysis, M2 macrophages were treated with PBS, HMW-HA, or LMW-HA for 24 h. For the blockade of TLR4,

macrophages were pretreated with 20 μg/mL anti-TLR4 antibody for 2 h prior to stimulation. To verify the status of macrophages polarization, total RNA was extracted from macrophages, and qRT-PCR was conducted with One Plus Step (Thermo Fisher, USA) and SYBR Premix (Takara, Japan) according to the manufacturer's instructions. The primer sequences of the relevant genes are listed in Supplementary Table 1.

2.11. Evaluation of the effects of Exos-PH20 on the tumor immune microenvironment of an orthotopic mouse model of breast cancer

An orthotopic mouse model of 4T1 breast tumor was established, and when the tumors reached 150–200 mm^3, mice were randomly separated into four groups: PBS, Exos-Con, Exos-PH20, and Exos-PH20-FA (5 mg/kg). Intra-tumoral injection was performed once every 2 days for 6 days. Six hours after the last measurement, mice were sacrificed. Tumors were isolated, cut into pieces, and then digested with DNase (Servicebio) and collagenase II (Yeasen, China) to prepare single-cell suspensions. Cells were blocked with an anti-Fc antibody and stained with fluorescence-labeled antibodies for CD45, CD11b, CD86, CD206, F4/80, CD3, CD4, CD8, and Foxp3 (Biolegend, USA) following the manufacturer's instructions. Immune cells were detected with a CytoFLEX flow cytometer and analyzed with FlowJo software. The intra-tumoral levels of IL-10 and IL-12 per 0.1 g tumor were detected with ELISA kits (Invitrogen) according to the manufacturer's instructions.

2.12. Assessment of the effects of Exos-PH20-FA on the migration of cancer cells in vitro

PC3 and 4T1 cancer cells were incubated in serum-free medium for 24 h. Next, 5×10^4 cells of each cell line were seeded into the top chamber of a Transwell with 100 μL serum-free medium supplemented with Exos-PH20-FA (100 μg/mL), as control, we added Exos-PH20, Exos-Con, PBS, and Exos-PH20 & free FA (10 μM).

The bottom chamber was filled with 500 μL medium supplemented with 10% FBS. After 24 h, the cells that migrated to the lower surface of the membrane insert were fixed in 4% paraformaldehyde and stained with 0.05% crystal violet. Three fields were randomly chosen, and the cells in each field were counted.

After reaching confluency, PC3 cells were mitotically inactivated with mitomycin C (5 mg/mL) for 2h to eliminate interference due to differences in proliferation. Cells were incubated for 12h with PBS, Exos-Con, Exos-PH20,and Exos-PH20-FA (100 μg/mL) before scratches were made in the monolayer of each triplicate well. Images were captured at 0 and 48 h, and the reduction in the size of the scratched areas was determined by tracing the wound edges and quantifying the open wound area with ImageJ software (Bethesda, NIH, USA).

2.13. Evaluation of the effects of Exos-PH20-FA in an orthotopic mouse model of breast cancer metastasis

For the 4T1 orthotopic tumor metastasis model, 4T1(Luc) tumor cells (1.0×10^6 cells/100 μL PBS) were injected into the mammary glands of each BALB/c mouse as 2.7. subsection described. When tumors reached 150–200 mm^3, mice were divided into four groups (n = 4): PBS, Exos-Con, Exos-PH20,and Exos-PH20-FA. According to the metabolic kinetics of HA in PH20, we injected Exos-PH20-FA or Exos-PH20 (5 mg/kg) into the tumor once every 2 days for 6 days. Distant metastasis of tumor cells was observed by *in vivo* imaging system, at 7- and 14-days post-treatment. After the last observation, mice were sacrificed, and the lungs were harvested and stained with Bouin's solution or H&E, after which the metastatic nodules were observed and counted.

2.14. Evaluation of antitumor effects of Dox@Exos-PH20-FA in vivo

To evaluate the antitumor efficacy of Dox@Exos-PH20-FA *in vivo*, tumor-bearing mice were randomly divided into six groups (n = 5). Each group was intravenously injected with saline (G1), free Dox (G2), Dox@Exos-Con (G3), Dox@Exos-PH20 (G4), or Dox@Exos-PH20-FA (G5) (100 μg Dox/200 μg total exosome protein) when the tumor volume reached 70 mm^3. The treatment was repeated every 3 days for a total of five times, and tumor volumes were measured every 3 days. Mice with tumors exceeding 2000 mm^3 were sacrificed. After the last measurement, mice were sacrificed, and tumors were harvested and weighed. $CD3^+CD8^+$ and $CD3^+CD4^+$ lymphocytes were isolated from tumor and stained for flow cytometry. Moreover, tumor tissues were fixed in 4% paraformaldehyde and cut into sections for TUNEL, Dox and CD8, CD86, and CD206 immunofluorescence staining. Serum levels of IFN-γ and TNF-α were measured with corresponding ELISA kits (Invitrogen) according to the manufacturer's instructions. Lungs were harvested and fixed for section cutting and H&E staining.

2.15. Statistical analysis

The analyses were conducted using commercial software (Prism 7.0; GraphPad Software, USA). Statistical analysis was performed using Student's *t*-test for two groups and Oneway analysis of variance for more than two groups. The values were presented as mean ± standard deviation (SD). The statistically significant differences were considered for p value < 0.05 ($^*p < 0.05$, $^{**}p < 0.01$, $^{***}p < 0.001$)

3. Results and discussion

3.1. Characterization of the engineered exosomes

As PH20 presents a short half-life *in vivo*, PEGylation can be performed to significantly extend the stability of PH20 in circulation; however, PEGylation may also reduce the activity of PH20 [27]. Transfecting cells to express PH20 using genetic engineering techniques can produce PH20 exosomes that are more active than PEGylated PH20 or PH20 chemically crosslinked to nanoparticles [11]. DSPE-PEG-FA has excellent affinity with phospholipid bilayers of exosomes and was used to modify exosomes with FA by self-assembly. The self-assembly approach relies on noncovalent forces, making it a bio-friendly strategy that does not disturb the biological activity of the engineered exosomes. To generate PH20 exosomes, we transfected 293T cells with a plasmid designed to express full-length PH20 on the cell membrane [11] (Fig. 2A). PH20 expression in transfected 293T cells was observed on the cell surface through immunofluorescence staining (Fig. 2B). We isolated the PH20-modified exosomes (Exos-PH20) from cell culture supernatants by serial centrifugation and ultracentrifugation. To conjugate FA with Exos-PH20, we mixed DSPE-PEG-FA, a pegylated phospholipid product with excellent amphiphilic properties that promotes the self-assembly of FA with Exo-PH20 to generating FA-modified Exos-PH20 (Exos-PH20-FA).

Exos-PH20-FA were characterized by Nano-Zetasizer, western blotting, TEM, and FTIR spectrometer. TEM revealed that Exos-PH20-FA (Fig. 2C), unmodified control exosomes (Exos-Con), and Exos-PH20 (Fig. S1) were round and approximately 100 nm in diameter. Western blotting analysis showed that Exos-PH20 and Exos-PH20-FA were both positive for PH20 and the exosomal marker proteins CD63 and CD9 (Fig. 2D). By comparing the size of the Exos-Con, Exos-PH20, and Exos-PH20-FA through dynamic light scattering analysis, we found that the diameter of Exos-PH20-FA was slightly increased, indicating that the incorporation of FA into the exosomal membrane did not significantly influence the exosome size (Fig. 2E). Furthermore, the 1413.2 and 1607.5 cm^{-1} absorption bands in the FTIR spectra supported the existence of benzoic vibrations and aromatic ring stretching vibrations with the integration of FA on the surface of Exos-PH20-FA [28] (Fig. 2F). Then, PH20 was serially diluted to generate reference standards to quantify the hyaluronidase activity by the turbidimetric assay, which showed an activity of 1971 and 2004 U/mg for Exos-PH20 and Exos-PH20-FA, respectively (Fig. 2G). These data demonstrate that Exos-PH20 and Exos-PH20-FA present high basal enzymatic activity, as previously reported [11], and the incorporation of FA

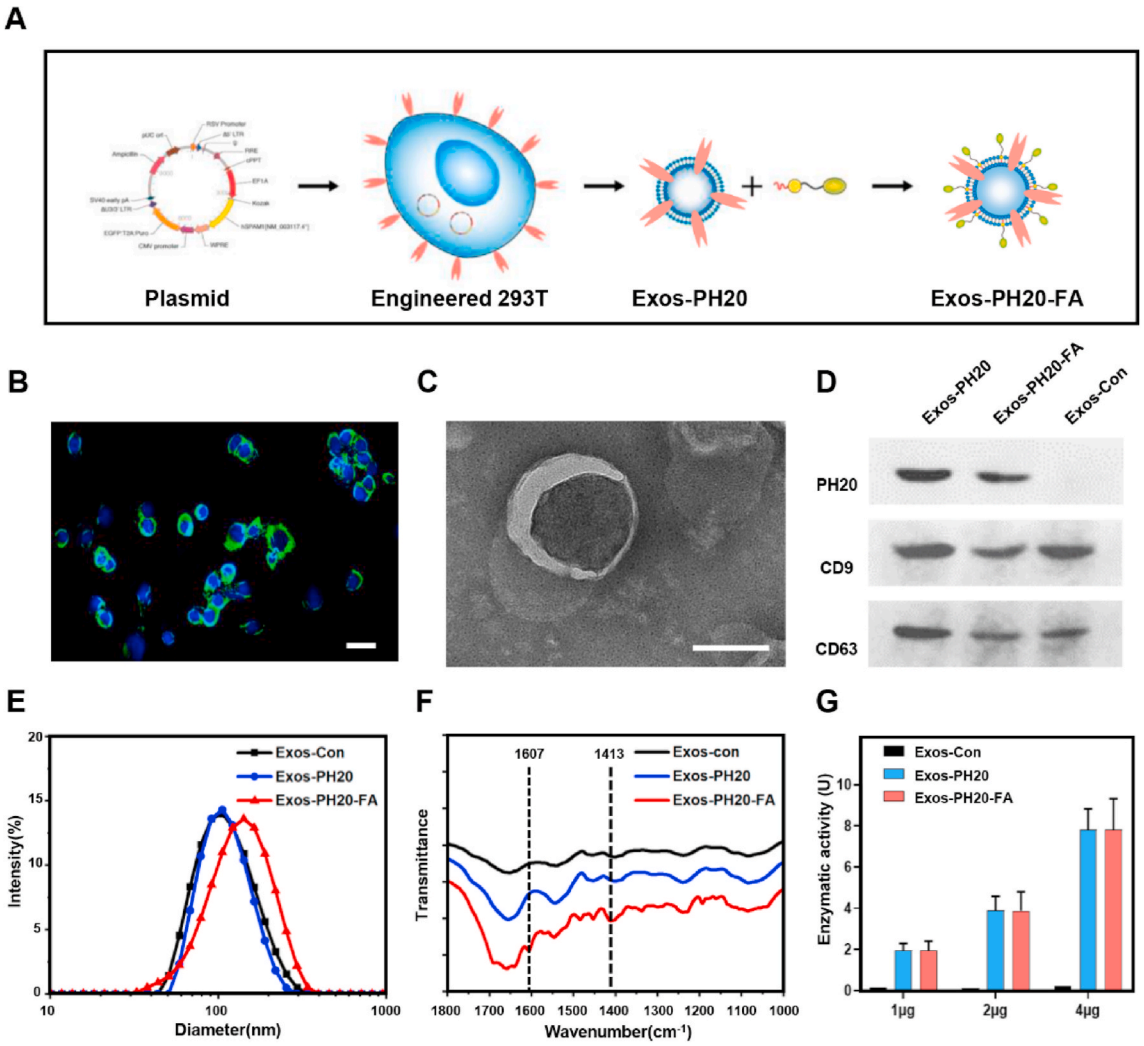

Fig. 2. A) Schematic diagram of the generation of exosomes derived from genetically engineered cells. B) Immunofluorescence of PH20 on the surface of plasmid-transfected 293T cells. Scale bar: 50 μm. C) TEM micrograph of Exos-PH20-FA. Scale bar: 100 nm. D) Western blotting analysis of PH20, CD9, and CD63 in the engineered exosomes. E) Hydrodynamic diameter of Exos-Con, Exos-PH20, and Exos-PH20-FA. F) FTIR analysis of Exos-Con, Exos-PH20, and Exos-PH20-FA. G) Hyaluronidase activity of different doses of Exos-Con, Exos-PH20, and Exos-PH20-FA. The data represent the mean ± SD.

into these exosomes did not perturb PH20 activity. Thus, self-assembly is a bio-friendly strategy for modifying engineered exosomes.

3.2. Evaluation of the enzymatic and tumor-targeting effects of Exos-PH20-FA in vitro and in vivo

Since the accumulation of HA in a wide range of solid tumors is related to poor survival rates, we next used 4T1 and PC3 cells as representative high HA-expressing tumor cell lines [11,21]. We observed more accumulation of pericellular HA in 4T1 and PC3 cells compared with HK-2 cells, which were selected as the non-malignant cells control group. Cultured cells were treated with 20 μg/mL Exos-Con, Exos-PH20, or Exos-PH20-FA for 4 h. The treatment with Exos-PH20 or Exos-PH20-FA reduced the HA levels in both PC3 and 4T1 cells, but no distinct effect was observed in the Exos-Con group. Furthermore, we observed obvious internalization of Exos-PH20 and Exos-PH20-FA by tumor cells (Fig. S2). However, there were fewer Exos-PH20-FA internalized in HK-2 cells because of the low expression of folate receptors. Since folate receptors are the target of FA-modified DDS for cancer therapy, the incorporation FA into exosome-based DDS, leads to a more effective internalization of exosomes by tumor cells. Compared with previously reported Exos-PH20 [11], Exos-PH20-FA exert better tumor-targeting effect, ensuring that sufficient PH20 can be supplied to the tumor tissue.

To assess tumor targeting *in vivo*, we used an orthotopic mouse model of breast cancer to determine the biodistribution of DiR-labeled Exos-Con, Exos-PH20, and Exos-PH20-FA. As shown in Figs. S3A and B, the fluorescence intensity at the tumor site was significantly higher in the Exos-PH20-FA group than in the Exos-PH20 or Exos-Con groups, indicating that FA-modified engineered exosomes are an effective delivery system. To evaluate the effect of enzymatically engineered exosomes on tumor ECM remodeling, we performed SEM to observe structural changes within subcutaneous tumors treated with Exos-Con, Exos-PH20, or Exos-PH20-FA. We found that Exos-PH20 and Exos-PH20-FA significantly alleviated the excessively dense ECM in the TME (Fig. S4A). Furthermore, we demonstrated by immunofluorescence that Exos-PH20 and Exos-PH20-FA significantly reduced HA, the major contributor for over-dense ECM, within the tumor (Fig. S4B). These results demonstrate that PH20 engineered exosomes can improve the TME, which is beneficial to the reduction of the intra-tumoral fluid pressure and elevation of drug perfusion [10]. Furthermore, Exos-PH20-FA were proven to exert the enzymatic activity of PH20 and the tumor-targeting ability of FA; the combination of these effects can improve TME more effectively.

3.3. Uptake of drug loaded exosomes inhibited tumor cell viability

Exos-PH20-FA not only improve TME but can also deliver

encapsulated chemotherapeutics to tumor cells. To confirm that the engineered exosomes can act as a tumor-targeting DDS, we treated 4T1 cells with various concentrations of free Dox and encapsulated Dox into Exos-Con, Exos-PH20, and Exos-PH20-FA. First, we assessed the efficiency of Dox encapsulated in Exos-PH20-FA. UV–vis absorption results indicated that as the concentration of Dox increased, the encapsulation efficiency grew slowly and finally reached at a plateau (Fig. S5). The MTT assay results showed that Exos-PH20-FA without drugs had no effect on cell growth, indicating its excellent biocompatibility, whereas Exos-PH20-FA encapsulating Dox (Dox@Exos-PH20-FA) significantly decreased the cytoactivity of 4T1 cells relative to the free Dox group (Dox $<$ 400 ng) (Fig. S6). To further explore if inhibited viability of cancer cell was due to the uptake of Dox@Exos-PH20-FA, we assessed the intracellular levels of Dox by flow cytometry. We found that 4T1 cells incubated for 6 h with Dox@Exos-PH20-FA (4 μg/mL Dox) internalized more Dox than those subjected to the other treatments (Fig. S7). These data indicate that Dox@Exos-PH20-FA efficiently target 4T1 cells and deliver Dox to the cell interior, thus inhibiting cell viability.

3.4. Immunosupportive response in the TME induced by HMW-HA degradation with PH20

Excessive HA has been related aggressive malignant tumors in patients or preclinical models. In breast cancer patients, the accumulation of HMW-HA is often accompanied by poor prognosis and high mortality [29]. Moreover, the accumulated HMW-HA can aggregate into cable-like structures that recruit macrophages, which are polarized to the pro-tumorigenic M2-like phenotype [30–32]. Hence, excessive HA leads to intra-tumor immunosuppression and prevents the efficacy of immunotherapy. Since Exos-PH20 and Exos-PH20-FA were found to degrade the HA secreted by HA^{hi} tumor cells, we used Mass Spectrometer analysis to measure the size of the HA degradation fragments and found that LMW-HA mainly included disaccharides and tetrasaccharides (Fig. S8). HMW-HA is a glycosaminoglycan composed of repeating disaccharides of N-acetyl-D-glucosamine and glucuronic acid linked by a glucuronidic β(1–3) bond; when degraded by hyaluronidases, the hexosaminidic β(1–4) linkages are cleaved, resulting in LMW-HA [33]. LMW-HA is a DAMP and can act as an immune response activator when ECM is damaged. Thus, we generated M2 macrophages by pretreating BMDMs with IL-4 for 24 h to investigate whether LMW-HA, degraded by Exos-PH20-FA of HMW-HA, could reprogram M2 macrophages to the M1 type (Fig. 3. A). Our results revealed that LMW-HA re-educated M2 toward M1 macrophages, as indicated by the inhibited expression of M2 relevant genes (IL-4, IL-10) and high expression of M1 relevant genes (IL-6, TNF-α) (Fig. 3B). Furthermore, we found that the blockade of TLR4 function inhibited the polarization of macrophages, which supported the involvement of TLR4 in LMW-HA-induced macrophage polarization also described in previous report [34,35]. Thus, we confirm that LMW-HA generated by hyaluronidase treatment can re-educate macrophages from the M2 to the M1 type.

Furthermore, *in vivo* experiments showed that PH20-mediated degradation of HA in 4T1 (HA^{hi}) tumors results in the establishment of an immunosupportive phenotype, as indicated by the higher numbers of M1-like TAMs and reduced numbers of M2-like TAMs (Fig. 3C). The macrophage polarization was also corroborated by the increased level of IL-12 and reduced level of IL-10, which are predominantly secreted by M1 and M2 macrophages, respectively, within the tumor (Fig. 3D). This of macrophage polarization to the M1 phenotype was not observed in the PBS or Exos-Con treated groups, which was ascribed to the PH20-induced HMW-HA degradation in the TME. The transformation of the immune microenvironment was also accompanied by a reduction in immunosuppressive cells associated with M2-like TAMs, such as Tregs (Fig. 3E and Fig. S9A). Correspondingly, the number of tumor-infiltrating lymphocytes ($CD3^+$), especially those of cytotoxic T lymphocytes ($CD3^+$ $CD8^+$), increased within the tumor (Fig. 3E and Figs. S9B and C). Compared to additional drugs that promote M1 polarization of TAMs [36], the Exos-PH20-FA mediated degradation of HA within the TME provides a simple and multiple-effect approach. Our results confirm that the HMW-HA scavenging by PH20 and generation of LMW-HA significantly affects the TME in HA^{hi} tumors, relieving an immunosuppressive state in tumor immunotherapy.

3.5. Exos-PH20-FA suppressed PH20-Triggered migration of tumor cells in vitro and in vivo

In solid tumors, the ECM constitutes a scaffold that supports and directs the migration of tumor cells [37]. We demonstrated that PH20 reduced the density of the ECM in tumors expressing high levels of HA and remodeled the TME, improving the antitumor therapeutic effect; however, the HA perturbation in ECM remodeling can also increase tumor cell migration [17]. The heterogeneity of the tumor microenvironment renders the complete killing of tumor cells by chemotherapy difficult. In turn, the metastasis of surviving drug-resistant tumor cells is triggered by hyaluronidase, contributing to a negative effect on prognosis. FA can not only modify the DDS to improve tumor targeting, but also inhibit the migration of cells without affecting cell viability by FA receptor/cSrc-signaling pathway [22,38]. Therefore, we modified our DDS with FA by a self-assembly approach using DSPE-PEG-FA and Exos-PH20 and found that the modified exosomes significantly inhibited hyaluronidase-induced metastasis (Fig. 4A). The Transwell assay showed that Exos-PH20 significantly increased the migration of tumor cells, but the Exos-PH20-FA-treated group was characterized by lower tumor cell migration (Fig. 4B). To evaluate whether the free FA cloud suppressed PH20-triggered migration of tumor cells, we compared the migration of PC3 and 4T1 cells treated by Exos-PH20 and Exos-PH20 & free FA. We observed the migration of combined group was significantly inhibited, indicating that free FA could also inhibited the tumor cell migration caused by hyaluronidase (Fig. S10). It was consistent with the previous reports that FA could inhibit cell migration [22,38]. In addition to the analysis of the vertical migration of tumor cells, we performed scratch assays to evaluate the effect of Exos-PH20-FA on the horizontal migration of PC3 cells. Exos-PH20-treated PC3 cells showed an increased rate of scratch closure, however, there was no significant difference in the cell migration rate between the PBS, Exos-Con, and Exos-PH20-FA-treated groups, and both scratch closure rates were lower than that in the Exos-PH20-treated group (Fig. 4C). These results suggest that Exos-PH20 increase the migration of tumor cells and the FA modification alleviates this phenomenon.

Furthermore, we investigated whether the FA modification inhibited Exos-PH20-triggered tumor cells metastasis *in vivo*. To this end, we used an orthotopic 4T1 (Luc) tumor metastasis model due to its extensive use in previous studies [39,40](Fig. 5A). The results revealed that 4T1(Luc) cells metastasized to the lungs in some mice of the Exos-PH20 group after 7-days post-treatment. However, the same trend was not observed in the Exos-PH20-FA group. After 14-days post-treatment, we detected tumor cell metastases in the lungs of all mice of the Exos-PH20 group, a higher number than that in the PBS, Exos-Con, and Exos-PH20-FA groups (Fig. 5B).

We also observed the metastatic nodules in the lung of each mouse and found that this number in mice treated with Exos-PH20-FA was significantly lower than that in the Exos-PH20 group (Fig. 5C). H&E staining of the lungs also revealed that the Exos-PH20 group showed obvious metastatic nodules (Fig. 5D). To investigate whether the different sizes of the primary tumors affected lung metastases, we calculated the size of primary tumors and found that Exos-PH20 and Exos-PH20-FA significantly limited the tumor volume, but the number of lung metastatic lesions was higher in the Exos-PH20 group than in the control group (Fig. 5E). Traditionally, the tumor volume is a risk factor for metastasis, with larger tumors often associated with a higher metastases risk. Nevertheless, some therapeutic interventions can break this relationship [20]. For instance, TME improvement by vascular

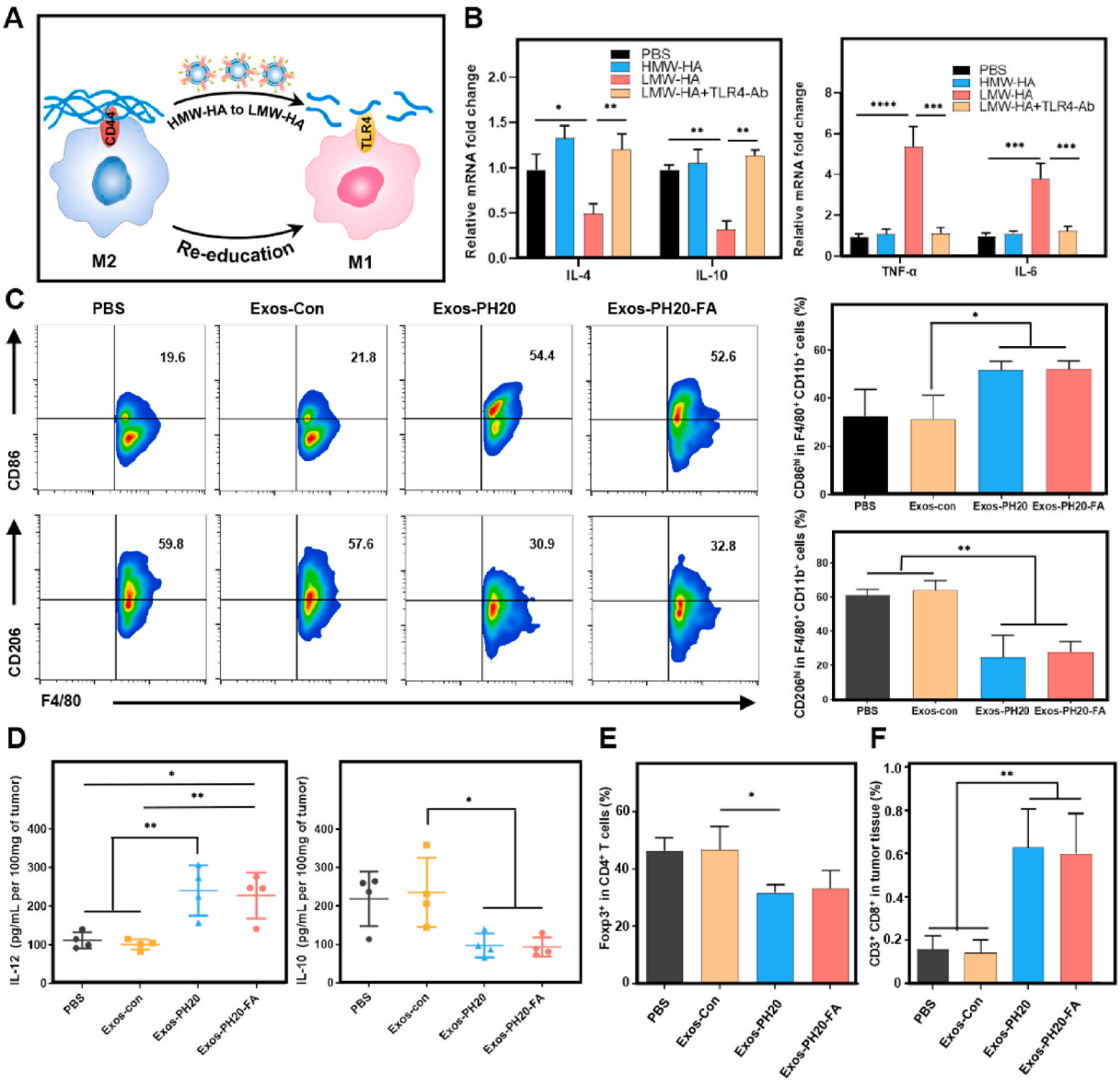

Fig. 3. A) Schematic illustration of re-education effects of LMW-HA, degraded by Exos-PH20-FA, on M2-like macrophage. B) Relative mRNA expressions of M2 markers (IL-4, IL-10) and M1 markers (TNF-α and IL-6) in M2 macrophages of administration with HMW-HA, LMW-HA, or LMW-HA + TLR4-Ab after 24 h, as compared to the control group (M2 macrophages only, group PBS). Data are presented as the mean ± SD. (n = 3, $*p < 0.05$, $**p < 0.01$, $***p < 0.001$, $****p < 0.0001$). C) Representative flow cytometric analysis images (left) and relative quantification (right) of M1-like macrophages ($CD86^{hi}$) and M2-like macrophages ($CD206^{hi}$) gating on $F4/80^+CD11b^+$ cells. Data are presented as the mean ± SD. (n = 3, $*p < 0.05$, $**p < 0.01$). D) Secretion levels of IL-12 (left) and IL-10 (right) in the tumors treated by PBS, Exos-Con, Exos-PH20, or Exos-PH20-FA. Data are presented as the mean ± SD. (n = 4, $*p < 0.05$, $**p < 0.01$). E) Flow cytometric quantification analysis of $CD4^+Foxp3^+$ T cells gating on $CD3^+CD4^+$ cells in the tumor and F) of $CD3^+CD8^+$ T cells in the tumor. Data are presented as the mean ± SD. (n = 3, $*p < 0.05$, $**p < 0.01$).

normalization effectively suppressed the tumor volume of primary sites, but increased the risk of tumor metastasis [19]. Our results suggest that Exos-PH20 exert complex actions on the tumor behavior, which limit primary tumor growth, but simultaneously may facilitate lung metastasis. In summary, Exos-PH20 can promote the metastasis of tumor cells through ECM remodeling, but the modification of Exos-PH20 with FA can alleviate it. The resulting Exos-PH20-FA not only target tumors, but also compensate for the side effects caused by PH20, making them an ideal DDS for hyaluronidase treatment of the TME.

3.6. Antitumor effects of Dox@Exos-PH20-FA in vivo

Inspired by the antitumor effects observed *in vitro*, we next evaluated the cooperative antitumor effects of immunotherapy and chemotherapy *in vivo* mediated by Dox@Exos-PH20-FA (Fig. 6A). 4T1 tumor-bearing BALB/c mice were randomly divided into five groups and intravenously injected with therapeutic agents. As shown in Fig. 6B, compared to mice treated with saline (G1), the free Dox group(G2) failed to exhibit tumor development, and only the Dox@Exos-Con (G3) groups displayed minor antitumor therapeutic effects may because of the enhanced permeability and retention effect. The Dox@Exos-PH20 (G4) group exhibited significant tumor growth inhibition, which can be explained by the TME improvement and better tumor perfusion of Dox. More importantly, the Dox@Exos-PH20-FA (G5) group exhibited significantly better therapeutic efficacy than that of the G4 group. The reduction in tumor weight among the different groups was consistent with the changes in tumor size (Fig. 6C). Fluorescent images showed a stronger Dox fluorescence in the tumors of mice treated with Dox@Exos-PH20-FAs but not in other groups (Fig. S11). The tumor-targeting effect of FA and its capacity to penetrate deeply into the tumor upon HA degradation ensures higher Dox release inside the tumors. Our results

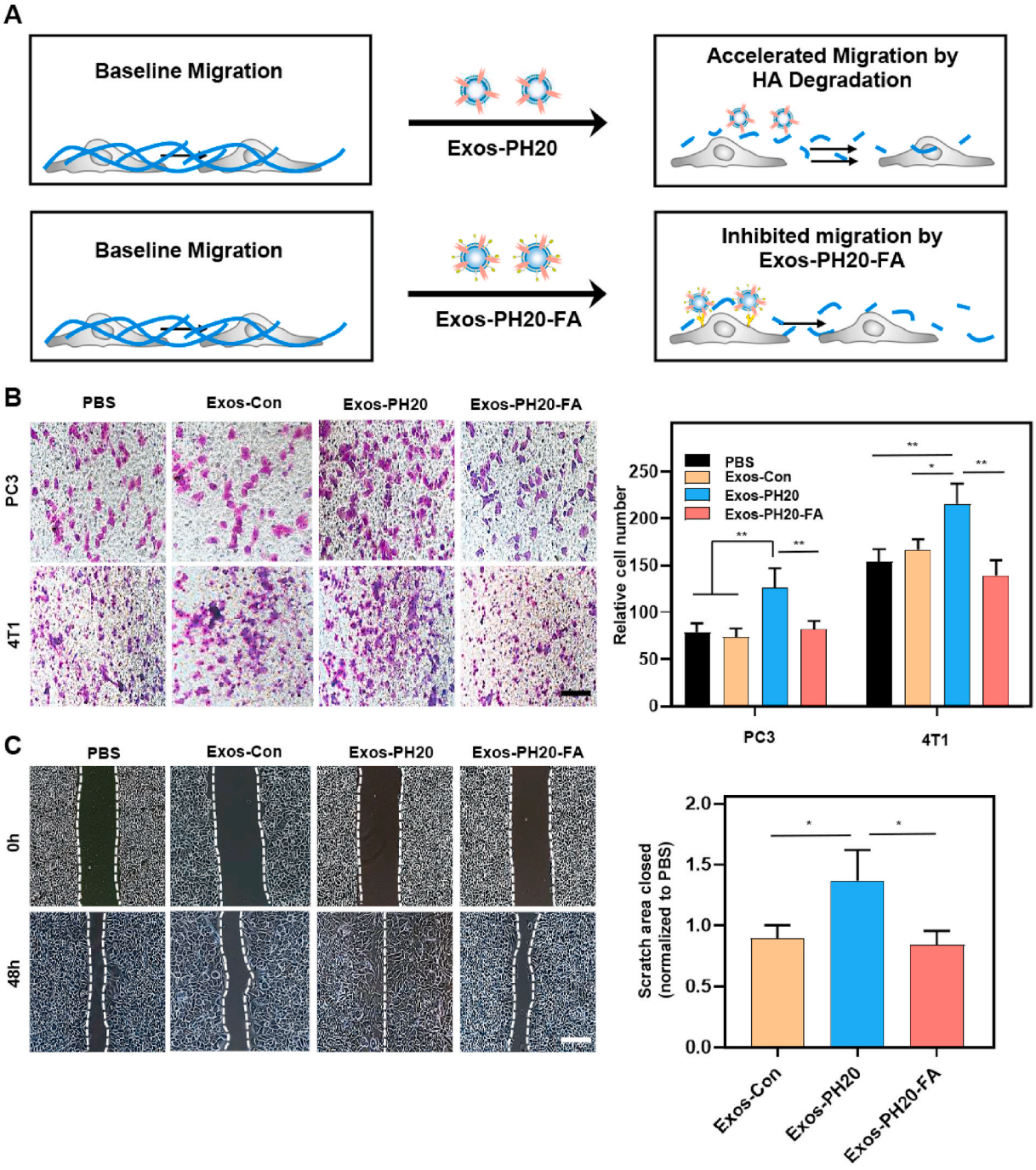

Fig. 4. A) Schematic illustration of Exos-PH20-FA inhibit the migration of cancer cells triggered by Exos-PH20. B) Transwell assay for PC3 and 4T1 cells treated with PBS, Exos-Con, Exos-PH20, or Exos-PH20-FA and relative quantification cell number. Data are presented as the mean ± SD (n = 3, $*p < 0.05$). Scale bar: 200 μm. C) Scratch assay showing the area closed by PC3 cells after treatment with PBS, Exos-Con, Exos-PH20, or Exos-PH20-FA. Representative images and relative quantification of closed scratch area. Data are presented as the mean ± SD (n = 3, $**p < 0.01$). Scale bar: 200 μm.

demonstrate that the Dox@ Exos-PH20-FA treatment effectively suppressed HA^{hi} 4T1 tumors. Furthermore, Dox@Exos-PH20-FA changed the immune microenvironment from immunosuppressive to immunosupportive. We assessed the level of TNF-α and INF-γ in the serum, as these cytokines are critical for tumor suppression and play vital roles in modulating immune activation [41]. We found that INF-γ and TNF-α was higher in the G4 and G5 groups than in the other control groups (Fig. 6D). We also observed a higher ratio of $CD3^+CD8^+$ (Fig. 6E) and $CD3^+CD4^+$ (Fig. S12) lymphocytes in G4 and G5 tumor tissues by flow cytometry. Moreover, immunohistochemical staining suggested that more $CD8^+$ cells infiltrated the tumors in the G4 and G5 groups (Fig. 6F). The higher immunofluorescent expression of CD86 and reduced CD206 in the G4 and G5 compared with control groups, which meant reeducation of M2-like TAMs to M1-like TAMs by hyaluronidase treatment (Fig. S13). This indicates that PH20 can significantly reverse the immunosuppressive state of the TME, allowing the infiltration of more immune cells and inflammatory factors with tumor-killing effects. On one hand, Dox@Exos-PH20-FA exert the tumor-targeting effect of FA, enabling the effective accumulation of Dox and PH20 in tumor foci. On the other hand, the PH20-induced TME modification also increases the ability of Dox to penetrate deeply into the tumor. The combination of these two effects significantly enhances the response to chemotherapy. Finally, achieving a cooperative effect of immunotherapy and

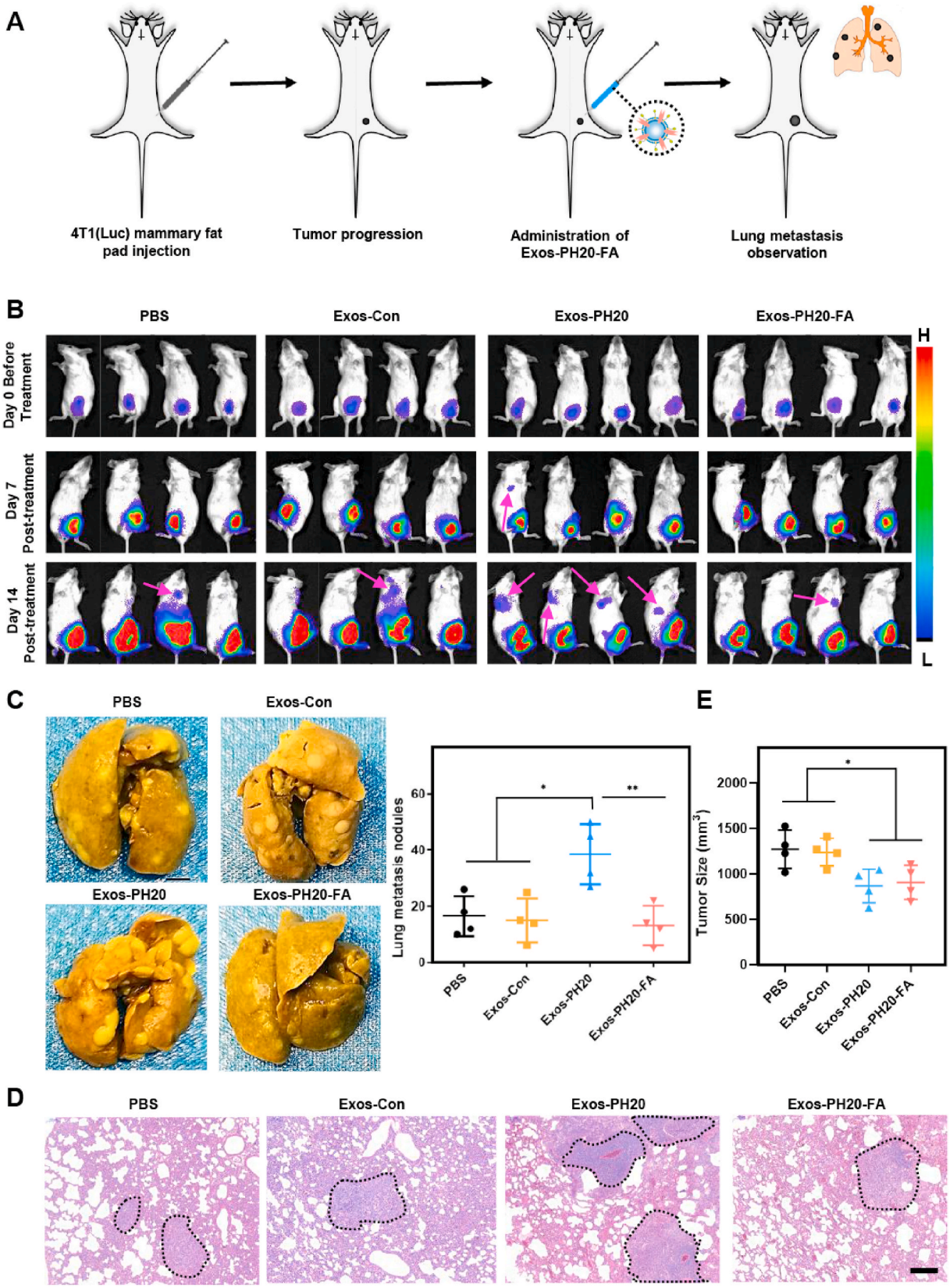

Fig. 5. A) Schematic of the breast cancer metastasis model with Exo-PH20-FA local treatment. B) Bioluminescence images of lung metastatic sites of 4T1(Luc) tumors after the administration of PBS, Exos-Con, Exos-PH20, or Exos-PH20-FA. The red arrow indicates the metastatic sites. C) Representative images of lungs collected from mice in the different groups at day 14 after treatment, the nodules indicate metastatic tumors in the lungs (left)and the quantitative analyses of macroscopically visible breast cancer metastases in the lungs(right). Data are presented as the mean ± SD (n = 4, $*p < 0.05$, $**p < 0.01$). D) H&E staining of lung metastatic sites of 4T1(Luc) tumors. Black borders indicate the metastatic sites. Scale bar: 200 μm. E) Quantitative analyses of primary tumor size. Data are presented as the mean ± SD (n = 4, $*p < 0.05$, $**p < 0.01$). (For interpretation of the references to colour in this figure legend, the reader is referred to the Web version of this article.)

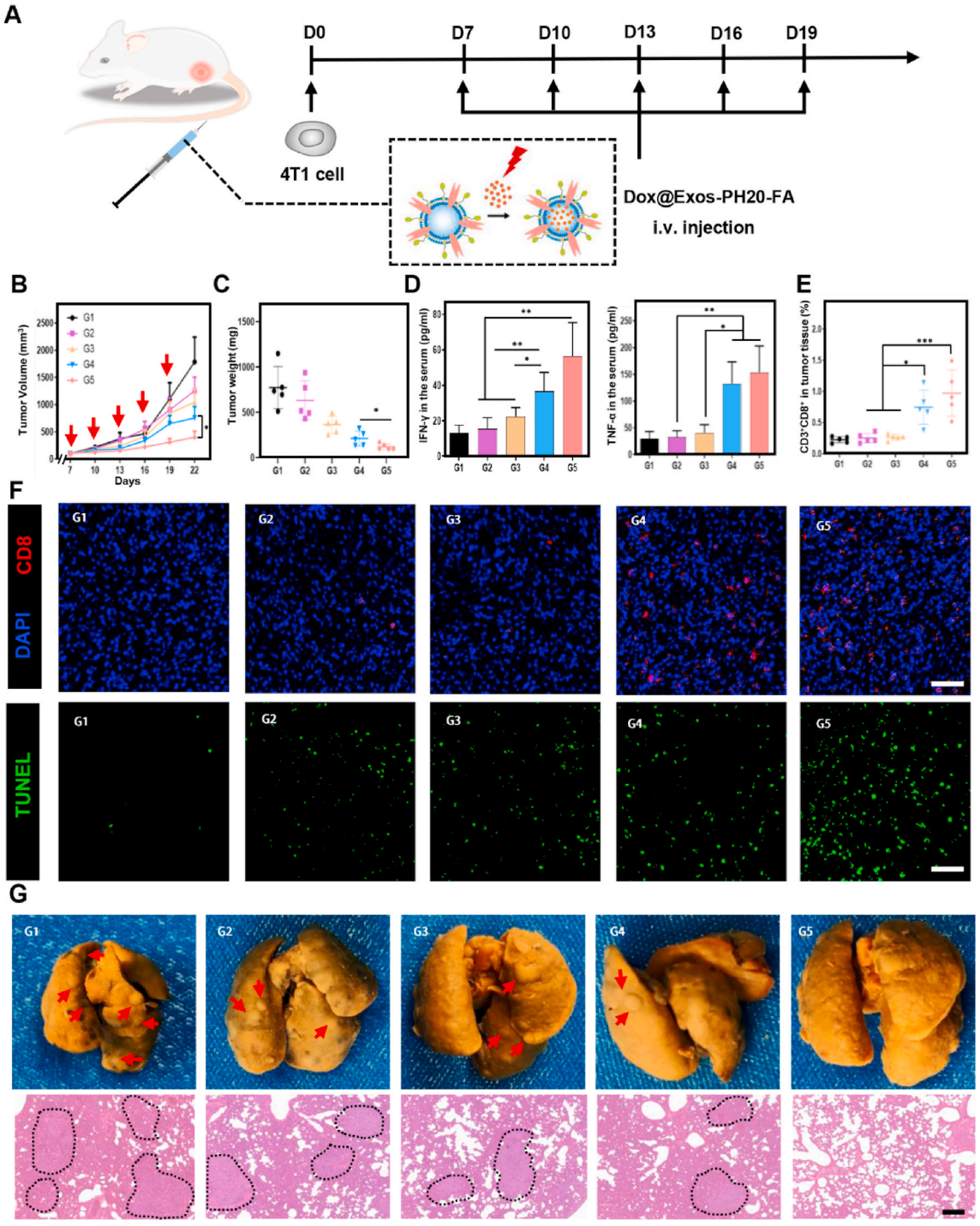

Fig. 6. A) Schematic illustration of Dox@Exos-PH20-FA intravenous injection therapy in a mouse breast cancer model. B) Tumor growth curves of mice from different groups. G1: Saline, G2: Free Dox, G3: Dox@Exos-Con, G4: Dox@Exos-PH20, G5: Dox@Exos-PH20-FA. (n = 5, $*p < 0.05$). C) Weight of tumors collected from mice 15 days after the first treatment. Data are presented as the mean ± SD (n = 5, $*p < 0.05$). D) Levels of serum INF-γ (left) and TNF-α (right) in the different groups. Data are presented as the mean ± SD (n = 5,$*p < 0.05$, $**p < 0.01$). E) Flow cytometric quantification analysis of $CD3^+CD8^+$T cells in the tumor tissue. Data are presented as the mean ± SD (n = 5, $*p < 0.05$, $***p < 0.001$). F) Representative immunofluorescence images showing tumor-infiltrating $CD8^+$T cells in 4T1 tumors in the different groups(up), and images showing TUNEL expression in the different groups(down). Scale bar: 50 μm. G) Representative images and H&E staining of metastatic sites of lungs from mice in the different groups. Red arrow and black borders indicate the metastatic sites. Scale bar: 200 μm. (For interpretation of the references to colour in this figure legend, the reader is referred to the Web version of this article.)

chemotherapy, the G5 group treated with Dox@Exos-PH20-FA showed the most significant tumor growth inhibition. The TUNEL assay also revealed that the Dox@Exos-PH20-FA treatment induced the highest tumor cell apoptotic rate among all groups (Fig. 6F). The ability of improving the TME and targeting the tumor showed by Dox@Exos-PH20-FA endows these exosomes with a more effective antitumor effect against HA^{hi} tumors. Furthermore, we found that no lung metastasis occurred in the Dox@Exos-PH20-FA group. However, compared with the control groups, Dox@Exos-PH20 group showed fewer tumor metastases, which may be related to PH20-induced more Dox perfusion in the tumor (Fig. 6G). In general, Dox@Exos-PH20-FA had effective anti-tumor and anti-metastasis effects *in vivo*.

4. Conclusion

In summary, to reverse the intra-tumoral immunosuppression microenvironment and the side effects of hyaluronidase treatment on HA^{hi} tumors, we developed a new exosome-based approach for improving cancer treatment by modulating the TME via hyaluronidase and FA modification. The tumor targeting effect of FA and HA degradation by hyaluronidase improved the efficacy of chemotherapy. Through ECM remodeling by hyaluronidase, the immunosuppressive phenotype in the TME weas relieved, which increased the infiltration of T cells and inflammatory factors with tumor cell-killing effect in the tumor. Moreover, combined chemotherapy and immunotherapy strategies may overcome the limitations of monotherapy, which often fails to achieve complete tumor remission. The FA modification inserted into the exosomes inhibited the migration of cancer cells caused by hyaluronidase-induced HA degradation, which can negatively impact the therapeutic efficacy of cancer treatment. This novel treatment strategy offers an innovative solution for overcoming the side effects of ECM degradation, combining immunotherapy activated and chemotherapy enhanced by targeted delivery.

CRediT authorship contribution statement

Chunxiang feng: Conceptualization, Methodology, Software, Writing - original draft, preparation. **Zhiyong Xiong:** Validation, Formal analysis, Visualization, Software. **Cheng Wang:** Writing - review & editing, Supervision, Data curation. **Wen Xiao:** Writing - review & editing, Supervision. **Haibing Xiao:** Validation, Formal analysis, Visualization. **Kairu Xie:** Data curation, Software, Validation. **Ke Chen:** Writing, Writing - review & editing. **Huageng Liang:** Writing - review & editing. **Xiaoping Zhang:** Resources, Writing - review & editing, Project administration. **Hongmei Yang:** Resources, Writing - review & editing, Project administration.

Declaration of competing interest

The authors declare that they have no known competing financial interests or personal relationships that could have appeared to influence the work reported in this paper.

Acknowledgments

This work was supported by: The National Key Research and Development Program of China (Grant No: 2017YFB1303100), The National Natural Science Foundation of China (Grant No: 81773282, 81972630, 81672528, 81874090), National Key Scientific Instrument and Equipment Development Project (Grant No: 81927807).

Appendix A. Supplementary data

Supplementary data to this article can be found online at https://doi.org/10.1016/j.bioactmat.2020.09.014.

References

[1] C.B. Thompson, H.M. Shepard, P.M. O'Connor, S. Kadhim, P. Jiang, R.J. Osgood, et al., Enzymatic depletion of tumor hyaluronan induces antitumor responses in preclinical animal models, MOL CANCER THER 9 (11) (2010) 3052–3064.
[2] R.H. Tammi, A. Kultti, V.M. Kosma, R. Pirinen, P. Auvinen, M.I. Tammi, Hyaluronan in human tumors: pathobiological and prognostic messages from cell-associated and stromal hyaluronan, SEMIN CANCER BIOL 18 (4) (2008) 288–295.
[3] D. Jiang, J. Liang, P.W. Noble, Hyaluronan as an immune regulator in human diseases, Physiol. Rev. 91 (1) (2011) 221–264.
[4] S.L. Kolar, P. Kyme, C.W. Tseng, A. Soliman, A. Kaplan, J. Liang, et al., Group B Streptococcus evades host immunity by degrading hyaluronan, Cell Host Microbe 18 (6) (2015) 694–704.
[5] H. Kim, J. Cha, M. Jang, P. Kim, Hyaluronic acid-based extracellular matrix triggers spontaneous M2-like polarity of monocyte/macrophage, Biomater Sci 7 (6) (2019) 2264–2271.
[6] Q. Shi, L. Zhao, C. Xu, L. Zhang, H. Zhao, High molecular weight hyaluronan suppresses macrophage M1 polarization and enhances IL-10 production in PM2.5-induced lung inflammation, Molecules 24 (9) (2019).
[7] M.I. Tammi, S. Oikari, S. Pasonen-Seppanen, K. Rilla, P. Auvinen, R.H. Tammi, Activated hyaluronan metabolism in the tumor matrix - causes and consequences, Matrix Biol. 78–79 (2019) 147–164.
[8] M.M. Rodríguez, E. Fiore, J. Bayo, C. Atorrasagasti, M. García, A. Onorato, et al., 4Mu decreases CD47 expression on hepatic cancer stem cells and primes a potent antitumor T cell response induced by interleukin-12, Mol. Ther. 26 (12) (2018) 2738–2750.
[9] S.R. Hingorani, L. Zheng, A.J. Bullock, T.E. Seery, W.P. Harris, D.S. Sigal, et al., Halo 202: Randomized phase II study of PEGPH20 plus nab-paclitaxel/gemcitabine versus nab-paclitaxel/gemcitabine in patients with untreated, metastatic pancreatic ductal adenocarcinoma, J. Clin. Oncol. 36 (4) (2018) 359–366.
[10] X. Li, H.M. Shepard, J.A. Cowell, C. Zhao, R.J. Osgood, S. Rosengren, et al., Parallel accumulation of tumor hyaluronan, collagen, and other drivers of tumor progression, CLIN CANCER RES 24 (19) (2018) 4798–4807.
[11] Y. Hong, G. Nam, E. Koh, S. Jeon, G.B. Kim, C. Jeong, et al., Exosome as a vehicle for delivery of membrane protein therapeutics, PH20, for enhanced tumor penetration and antitumor efficacy, Adv. Funct. Mater. 28 (17030745) (2018).
[12] H. Gong, Y. Chao, J. Xiang, X. Han, G. Song, L. Feng, et al., Hyaluronidase to enhance nanoparticle-based photodynamic tumor therapy, Nano Lett. 16 (4) (2016) 2512–2521.
[13] Y. Hong, Y.K. Kim, G.B. Kim, G. Nam, S.A. Kim, Y. Park, et al., Degradation of tumour stromal hyaluronan by small extracellular vesicle-PH20 stimulates CD103 + dendritic cells and in combination with PD-L1 blockade boosts anti-tumour immunity, J. Extracell. Vesicles 8 (1) (2019) 1670893.
[14] A. Mantovani, S. Sozzani, M. Locati, P. Allavena, A. Sica, Macrophage polarization: tumor-associated macrophages as a paradigm for polarized M2 mononuclear phagocytes, Trends Immunol. 23 (11) (2002) 549–555.
[15] Q. Chen, C. Wang, X. Zhang, G. Chen, Q. Hu, H. Li, et al., In situ sprayed bioresponsive immunotherapeutic gel for post-surgical cancer treatment, Nat. Nanotechnol. 14 (1) (2019) 89–97.
[16] O.R. Colegio, N.Q. Chu, A.L. Szabo, T. Chu, A.M. Rhebergen, V. Jairam, et al., Functional polarization of tumour-associated macrophages by tumour-derived lactic acid, Nature 513 (7519) (2014) 559–563.
[17] W.J. Sullivan, P.J. Mullen, E.W. Schmid, A. Flores, M. Momcilovic, M.S. Sharpley, et al., Extracellular matrix remodeling regulates glucose metabolism through TXNIP destabilization, Cell 175 (1) (2018) 117–132.
[18] C. Peng, M. Wallwiener, A. Rudolph, K. Cuk, U. Eilber, M. Celik, et al., Plasma hyaluronic acid level as a prognostic and monitoring marker of metastatic breast cancer, Int. J. Can. 138 (10) (2016) 2499–2509.
[19] M. Paez-Ribes, E. Allen, J. Hudock, T. Takeda, H. Okuyama, F. Vinals, et al., Antiangiogenic therapy elicits malignant progression of tumors to increased local invasion and distant metastasis, Canc. Cell 15 (3) (2009) 220–231.
[20] Y. Husaini, M.R. Qiu, G.P. Lockwood, X.W. Luo, P. Shang, T. Kuffner, et al., Macrophage inhibitory cytokine-1 (MIC-1/GDF15) slows cancer development but increases metastases in TRAMP prostate cancer prone mice, PloS One 7 (8) (2012) e43833.
[21] P. Jiang, X. Li, C.B. Thompson, Z. Huang, F. Araiza, R. Osgood, et al., Effective targeting of the tumor microenvironment for cancer therapy, Anticancer Res. 32 (4) (2012) 1203–1212.
[22] P.C. Ting, W.R. Lee, Y.N. Huo, S.P. Hsu, W.S. Lee, Folic acid inhibits colorectal cancer cell migration, J. Nutr. Biochem. 63 (2019) 157–164.
[23] S.C. Jang, O.Y. Kim, C.M. Yoon, D. Choi, T. Roh, J. Park, et al., Bioinspired exosome-mimetic nanovesicles for targeted delivery of chemotherapeutics to malignant tumors, ACS Nano 7 (9) (2013) 7698–7710.
[24] E.S. Choi, J. Song, Y.Y. Kang, H. Mok, Mannose-modified serum exosomes for the elevated uptake to murine dendritic cells and lymphatic accumulation, Macromol. Biosci. 19 (7) (2019) e1900042.
[25] W. Zhang, Z. Yu, M. Wu, J. Ren, H. Xia, G. Sa, et al., Magnetic and folate functionalization enables rapid isolation and enhanced tumor-targeting of cell-derived microvesicles, ACS Nano 11 (1) (2017) 277–290.
[26] K. Wang, D.S. Guo, X. Wang, Y. Liu, Multistimuli responsive supramolecular vesicles based on the recognition of p-Sulfonatocalixarene and its controllable release of doxorubicin, ACS Nano 5 (4) (2011) 2880–2894.
[27] P. Zucca, E. Sanjust, Inorganic materials as supports for covalent enzyme immobilization: methods and mechanisms, Molecules 19 (9) (2014) 14139–14194.
[28] C. Sun, R. Sze, M. Zhang, Folic acid-PEG conjugated superparamagnetic nanoparticles for targeted cellular uptake and detection by MRI, J. Biomed. Mater. Res. A 78 (3) (2006) 550–557.
[29] S. Tiainen, A. Masarwah, S. Oikari, K. Rilla, K. Hämäläinen, M. Sudah, et al., Tumor microenvironment and breast cancer survival: combined effects of breast fat, M2 macrophages and hyaluronan create a dismal prognosis, Breast Canc. Res. Treat. 179 (3) (2020) 565–575.
[30] T.A. Jokela, J. Kuokkanen, R. Karna, S. Pasonen-Seppanen, K. Rilla, J. Kossi, et al., Mannose reduces hyaluronan and leukocytes in wound granulation tissue and inhibits migration and hyaluronan-dependent monocyte binding, Wound Repair Regen. 21 (2) (2013) 247–255.
[31] D.M. Kuang, Y. Wu, N. Chen, J. Cheng, S.M. Zhuang, L. Zheng, Tumor-derived hyaluronan induces formation of immunosuppressive macrophages through transient early activation of monocytes, Blood 110 (2) (2007) 587–595.
[32] G. Zhang, L. Guo, C. Yang, Y. Liu, Y. He, Y. Du, et al., A novel role of breast cancer-derived hyaluronan on inducement of M2-like tumor-associated macrophages formation, OncoImmunology 5 (6) (2016) e1172154.
[33] D. Jiang, J. Liang, P.W. Noble, Hyaluronan in tissue injury and repair, Annu. Rev. Cell Dev. Biol. 23 (2007) 435–461.

[34] M. Sokolowska, L. Chen, M. Eberlein, A. Martinez-Anton, Y. Liu, S. Alsaaty, et al., Low molecular weight hyaluronan activates cytosolic phospholipase A2α and eicosanoid production in monocytes and macrophages, J. Biol. Chem. 289 (7) (2014) 4470–4488.
[35] M. Song, T. Liu, C. Shi, X. Zhang, X. Chen, Bioconjugated manganese dioxide nanoparticles enhance chemotherapy response by priming tumor-associated macrophages toward M1-like phenotype and attenuating tumor hypoxia, ACS Nano 10 (1) (2016) 633–647.
[36] C.B. Rodell, S.P. Arlauckas, M.F. Cuccarese, C.S. Garris, R. Li, M.S. Ahmed, et al., TLR7/8-agonist-loaded nanoparticles promote the polarization of tumour-associated macrophages to enhance cancer immunotherapy, Nat. Boimed. Eng. 2 (2018) 578–588.
[37] M.J. Oudin, O. Jonas, T. Kosciuk, L.C. Broye, B.C. Guido, J. Wyckoff, et al., Tumor cell-driven extracellular matrix remodeling drives haptotaxis during metastatic progression, Cancer. Discov. 6 (5) (2016) 516–531.
[38] T.C. Hou, J.J. Lin, H.C. Wen, L.C. Chen, S.P. Hsu, W.S. Lee, Folic acid inhibits endothelial cell migration through inhibiting the RhoA activity mediated by activating the folic acid receptor/cSrc/p190RhoGAP-signaling pathway, Biochem. Pharmacol. 85 (3) (2013) 376–384.
[39] D. Shan, L. Chen, J.T. Njardarson, C. Gaul, X. Ma, S.J. Danishefsky, et al., Synthetic analogues of migrastatin that inhibit mammary tumor metastasis in mice, Proc. Natl. Acad. Sci. U. S. A. 102 (10) (2005) 3772–3776.
[40] Y. Fang, Y. Chen, L. Yu, C. Zheng, Y. Qi, Z. Li, et al., Inhibition of breast cancer metastases by a novel inhibitor of TGFbeta receptor 1, J. Natl. Cancer Inst. 105 (1) (2013) 47–58.
[41] X. Guan, J. Chen, Y. Hu, L. Lin, P. Sun, H. Tian, et al., Highly enhanced cancer immunotherapy by combining nanovaccine with hyaluronidase, Biomaterials 171 (2018) 198–206.